Prediction of Rolling Bed Motion in Rotating Cylinders

Jochen Mellmann
Leibniz Institute of Agricultural Engineering, Potsdam-Bornim (ATB), D-14469 Potsdam, Germany

Eckehard Specht and Xiaoyan Liu
Institute of Fluid Mechanics and Thermodynamics, Otto-von-Guericke-University Magdeburg, D-39016 Magdeburg, Germany

DOI 10.1002/aic.10266
Published online in Wiley InterScience (www.interscience.wiley.com).

A mathematical model for the range of rolling bed motion has been developed to calculate the transverse solids motion in rotating cylinders. It is based on mass and momentum balances with physically specified and hence known initial conditions. The behavior of the bed material need only be described by two measurable parameters, the dynamic angle of repose and the angle of slope at the start of the boundary line (interface between the cascading layer and the plug flow region). The shape of the boundary line, the thickness of the cascading layer, the mass flow rate, and the velocity at the surface can be predicted as a function of rotation speed, filling degree, and cylinder diameter. No fitting parameter is needed for the calculation. To verify the model, experiments were carried out for many bed materials and rotating cylinder conditions. A correlation for the angle of slope at the start of the boundary line is given. The calculated results of the model are then compared to our own measurements and those reported in the literature. It is shown that the model agrees relatively well with the experiments. © 2004 American Institute of Chemical Engineers *AIChE J,* 50: 2783–2793, 2004
Keywords: rotating cylinder, bed motion, rolling, particle velocity

Introduction

Rotating cylinders or rotary kilns are used to handle large throughputs in physical processes such as size reduction, agglomeration, mixing, drying, heating, cooling, as well as gas–solid chemical reaction and solid thermal decomposition. Many of these processes are controlled by solids transport and particulate mixing within the bed. Depending on the rotation speed and filling degree, several types of bed motions can be observed: slipping, slumping, rolling, cascading, cataracting, and centrifuging (Henein et al., 1983; Mellmann, 2001). Studies of the transition behavior of the bed motions have been reported, for example, by Rajchenbach (1990), Mellmann and Specht (2001), and Ding et al. (2002a).

Industrial rotary kilns are mostly operated at slumping or rolling mode because of their low rotation speed. At the slumping mode, the particles avalanche intermittently along the bed surface. As the rotation speed increases, the avalanches become continuous and rolling occurs, characterized by a thin layer of particles along a nearly flat bed surface (cascading layer), and a thicker layer rotating together with the kiln wall as a fixed bed (plug flow region). Kelbert et al. (1991) studied the mixing and heat transfer in a rolling bed and demonstrated that the mixing has a preponderant influence on the temperature distribution inside the solid bed. Boateng et al. (1996) reported that a rolling bed is better than a slumping bed in that its bed surface can be renewed more quickly, resulting in improved heat transfer. According to the recent work of Ding et al. (2001a), however, for rotary kilns operated at low to medium tempera-

Correspondence concerning this article should be addressed to X. Liu at xiaoyan.liu@student.uni-magdeburg.de.

tures, the rolling mode does not really help much to improve heat transfer, which is contrary to the previously held view. This reveals the complexity of the motion behavior and the necessity for further study. Theoretical models, however, should not be too complicated to be later coupled with heat transfer models.

Both theoretical and experimental efforts have been devoted to the bed motion in rotating cylinders. Recently, Orpe and Khakhar (2001) experimentally studied the flow of various materials in cylinders of different sizes. Results indicate that at low Froude numbers the bed surface is nearly flat and the layer thickness profile is symmetric (rolling motion). With increasing Froude number the surface becomes increasingly S-shaped (cascading motion). The scaled thickness of the cascading layer was found to increase with increasing Froude number and with an increase in size ratio d/D (particle diameter to cylinder diameter). Félix et al. (2002) measured the maximum thickness of the cascading layer in the range of rolling and cascading motion. The following conclusions were made: for large d/D ratios, the thickness of the cascading layer is determined by the geometry of the cylinder and it is nearly unaffected by the rotation speed, whereas for small d/D ratios, the thickness increases continuously with the rotation speed. Ding et al. (2002b) investigated the behavior of a rolling bed consisting of a mixture of small and large particles. It is shown that the bed structure for a binary mixture is similar to that for monosized particles. Bonamy et al. (2002) measured the velocity profile in the cascading layer at the center of the cylinder by using a fast camera. The velocity profile was found to be linear with a gradient independent of both the thickness and the local slope of the bed layer interface. Alexander et al. (2002) measured surface velocities of glass beads in half-filled rotating cylinders. Symmetric velocity profiles were observed at low Froude numbers (Fr = 0.0015 and Fr = 0.055 in the cylinder $D = 14.5$ cm). With increasing Froude number the profile becomes asymmetric (Fr = 0.22). Jain et al. (2002) experimentally studied the velocity field within the cascading layer using particle-tracking velocimetry. Most of the measurements in the literature used, however, involved a fixed filling degree of $f = 0.5$, which is much higher than filling degrees in industrial rotary kilns ($f = 0.05$–0.3).

The bed motion in rotating cylinders has also been extensively studied theoretically. In the earlier work of Perron and Bui (1992) a two-dimensional mathematical model was developed for the cascading motion by applying the Navier–Stokes equations to the material bed of the rotating cylinder. The partial differential equation system was solved with the aid of the CFD software package FLUENT. Various approaches, including that of Perron and Bui (1990), were compared with each other to model the bed rheology. However, these approaches are based on extremely simplifying assumptions. For instance, it is assumed that the residence time of a particle in the plug flow region is equal to the time in the cascading layer. In fact, however, the former is a multiple of the latter. Ferron and Singh (1991) and Kohav et al. (1995) provide equations for the residence time and velocity at the bed surface that neglect the important influence of rotational speed and particle size. More recently, several models were developed to describe the structure of the bed layer. Orpe and Khakhar (2001) reviewed them in detail and compared predictions of different models to their measurements. According to their report, predictions of models by Elperin and Vikhansky (1998) and Makse (1999) match well with the experimental data at low Froude numbers, where the bed profiles are symmetric. The continuum model of Khakhar et al. (1997) well describes the profiles of the cascading layer in a wide range of Froude numbers. However, all models require a fitting parameter, which is adjusted so that the calculated layer thickness matches the experimentally measured value. A review of these models will not be repeated in this work. Recently, Gray (2001) presented simple equations to calculate the bed layer profiles for steady flow. However, the downslope velocity of the particles is considered to be constant and its ratio to the angular velocity of the cylinder must be given for the calculation. Ding et al. (2002a) gave an equation for the maximum velocity at bed surface valid in the range of the Froude number $0.002 \leq \mathrm{fr} \leq 0.014$, which was derived from experimental results by correlation, however.

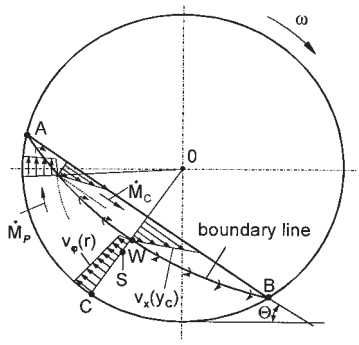

Figure 1. Mechanism of the rolling motion.

In this work we focus on the rolling motion, which is widely used in industrial rotary kilns. A mathematical model is developed based on the previous work of Mellmann (1989). It differs from the work in the literature in that the friction force at the interface between the cascading layer and the plug flow region is assumed to vary along the position and coefficient of friction is assumed to vary linearly with the distance along the cascading layer. Based on mass and momentum balances for the bed flow, a one-order differential equation predicting the position of the bed layer interface is derived and solved with physically specified initial conditions. No fitting parameter is needed. Parameters necessary for the model calculation are: cylinder diameter D, Froude number Fr, fill angle ε (filling degree f), and bed material properties including particle diameter d, dynamic angle of repose Θ, and the angle of slope ν_A. The angle ν_A is a characteristic angle of the cascading layer that can be measured directly or approximated by using the empirical equation obtained from our experiments. To verify the model, experiments were carried out in rotating cylinders involving several bed materials under different operating conditions (rotation speed and filling degree).

Mathematical Model

Bed motion

The rolling motion will be described in the following (see Figure 1). A uniform, static flow of a particle layer on the surface (cascading layer) is characteristic for rolling, whereas the larger part of the bed (plug flow region) is transported upward by solid body rotation with the rotational speed of the

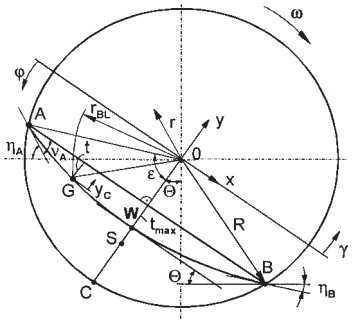

Figure 2. Coordinate system and influence variables.

wall in the case of adhesive friction. The bed surface is almost level and inclined toward the horizontal about the dynamic angle of repose Θ. The resulting flow profile is characterized by a vortex center (vortex point W) in the middle of the bed, which is located close to the mass center of gravity *S*. The interface between the cascading layer and the plug flow region is designated below as a boundary plane, and the transverse section through this plane as the boundary line. The latter extends from the top of the bed (point A) by the vortex point W to the foot of the bed (point B). Dilatation of the bed appears in a narrow volume segment along this line as a consequence of deflection of the particle tracks. Incipient flow occurs along the upper half of the boundary line (from the vortex point W to point A). Here particles become detached from the fixed particle arrangement of the plug flow region and are accelerated and entrained by particles of the cascading layer flowing over them. The circular particle tracks in the plug flow region transfer into particle tracks running parallel to the bed surface. There is now a reversal of motion at the boundary line in the lower half of the bed (from the vortex point W to point B), along which particles from the cascading layer line up in the plug flow region again. The particle velocity in the cascading layer v_x is a multiple of the velocity in the plug flow region v_φ. The thickness of the cascading layer increases toward the interior, starting at the rotating cylinder wall, and reaches its maximum $t_W = t_{max}$ roughly in the middle of the bed.

For a given filling degree the rolling motion can be reduced to a two-dimensional mathematical problem. The origin of the coordinate system selected lies in the cylinder axis (Figure 2). Taking into account the motion structures in the plug flow region and the cascading layer, both polar coordinates (r, γ) and Cartesian coordinates (x, y) are used, whereby x lies in the plane of the bed surface. For the rolling motion the Froude number Fr is relatively small and the bed surface is nearly level. It can be assumed that there is a symmetrical flow profile with respect to the line OC. Accordingly it is sufficient to observe only one half of the solid bed. The upper half of the bed is modeled below. The points on the boundary line are denoted with the subscript *BL*. The following connections exist on the line between the coordinates

$$x_{BL} = r_{BL}\cos\gamma \tag{1}$$

and

$$y_{BL} = r_{BL}\sin\gamma \tag{2}$$

As auxiliary coordinates the angle

$$\varphi = \gamma - \pi \tag{3}$$

and the length coordinate y_C of the cascading layer t are introduced in Figure 2 with $0 \le y_C \le t$. The angle φ is used below for representations in polar coordinates. Taking into account the distance between the bed and the cylinder axis, the local thickness of the cascading layer is calculated with Eqs. 2 and 3 to be

$$t = r_{BL}\sin\varphi - R\cos\varepsilon \tag{4}$$

The velocity, the mass flow rate, and the shape of the boundary line are calculated below.

Velocity and mass flow rate

At constant rotation speed the velocity in the plug flow region depends only on the radius of the particle track (Figure 1)

$$v_\varphi(r) = \omega r \tag{5}$$

The transverse velocity in the cascading layer is distributed roughly in linear fashion over the layer thickness with

$$v_x(y_C) = \frac{2\bar{v}_x}{t}\,y_C \tag{6}$$

as has been revealed so far by experimental studies in generally trickling beds (Boateng, 1993; Bonamy et al., 2002; Mellmann, 1989; Tscheng, 1978). The term $\bar{v}_x$ in Eq. 6 characterizes the mean velocity in the cascading layer. The transverse velocity at the level of the boundary line is equal to zero $v_x\,(y_C = 0) = 0$. The mean velocity in the cascading layer $\bar{v}_x$ can be determined from the mass flow balance.

The particle mass flow rates in the plug flow region and the cascading layer can be calculated when the shape of the boundary line $r_{BL}(\varphi)$ is known. (The calculation of the boundary line is the subject of the following section.) The mass flow rate related to the rotating cylinder length in the plug flow region is calculated as

$$\frac{\dot{M}_P}{L} = \rho_{b,P}\int_{r_{BL}}^{R} v_\varphi(r)\,dr \tag{7}$$

By integrating Eq. 7 with Eq. 5 we obtain

$$\frac{\dot{M}_P}{L} = \rho_{b,P}\,\frac{\omega}{2}\,(R^2 - r_{BL}^2) \tag{8}$$

The length-related mass flow rate in the cascading layer is calculated as

$$\frac{\dot{M}_C}{L} = \rho_{b,C} \int_0^t v_x(y_C)\, dy_C \tag{9}$$

and after integration with Eq. 6 we obtain

$$\frac{\dot{M}_C}{L} = \rho_{b,C} \bar{v}_x t \tag{10}$$

According to the principle of mass conservation the two mass flow rates

$$\dot{M}_C = \dot{M}_P \tag{11}$$

are equal at each point on the boundary line. The mean velocity in the cascading layer results after applying Eqs. 8 and 10 in Eq. 11 and reforming this from

$$\bar{v}_x = \frac{\rho_{b,P}}{\rho_{b,C}} \frac{\omega(R^2 - r_{BL}^2)}{2t} \tag{12}$$

In the rolling motion the bed is subjected to a periodic change between free, almost pressureless flow in the cascading layer and "consolidation" in the plug flow region. As a result of consolidation, the bed density $\rho_{b,P}$ in the plug flow region can be greater than the bulk density ρ_b of the reposing bed measured in the pressureless condition. In the cascading layer, on the other hand, the bed density $\rho_{b,C}$ can be lower because of dilatation. The consolidation stress in the bed of a large-scale industrial rotary kiln is relatively low, however, compared with that in silos and bunkers. Any increase or reduction of the bulk density in the plug flow region and cascading layer is neglected below with

$$\rho_{b,P} = \rho_{b,C} = \rho_b \tag{13}$$

The shape of the boundary line is needed with r_{BL} and t to calculate the velocity.

Boundary line

Geometric Connections. Figure 3a shows a differential element of the cascading layer dx_{BL} in the rotating cylinder cross section. Particles with a mean velocity $\bar{v}_x$ flow continuously through this element that touches the boundary line over a length of ds. The boundary line is inclined to the horizontal about the angle

$$\eta = \Theta + \nu \tag{14}$$

After passing the section dx_{BL} the cascading layer thickness has increased by the amount dt. This gradient is expressed by the angle of inclination ν of the boundary line to the level bed surface, which is thus calculated from

$$\tan \nu = \frac{dt}{dx_{BL}} = -\frac{dy_{BL}}{dx_{BL}} \tag{15}$$

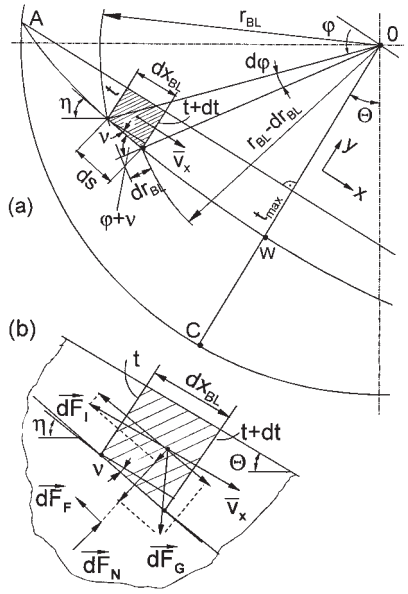

Figure 3. (a) Differential element of the cascading layer in the bed cross section. (b) Balance of forces.

The following relation exists between the path dx_{BL} and the section ds of the boundary line

$$\cos \nu = \frac{dx_{BL}}{ds} \tag{16}$$

whereas on the path dx_{BL} the cascading layer thickness has increased by the amount dt, at the same time the depth of the plug flow region in the radial direction has increased by the amount dr_{BL}. This connection is illustrated by

$$\frac{dr_{BL}}{dx_{BL}} = -\frac{\cos(\varphi + \nu)}{\cos \nu} \tag{17}$$

The shape of the boundary line can be represented in both Cartesian coordinates [$y_{BL} = y_{BL}(x_{BL})$] and polar coordinates [$r_{BL} = r_{BL}(\varphi)$]. The differential equation of the boundary line in Cartesian coordinates follows from Eq. 15 to

$$\frac{dy_{BL}}{dx_{BL}} = -\tan \nu \tag{18}$$

A representation in polar coordinates is selected below. By converting Eq. 18 with the aid of Eqs. 1 to 4 and trigonometric relations, we obtain the differential equation of the boundary line, according to Mellmann (1989), as

$$\frac{dr_{BL}}{d\varphi} - r_{BL} \frac{\tan \varphi \tan \nu - 1}{\tan \varphi + \tan \nu} = 0 \tag{19}$$

The initial condition will be discussed below separately. The increase in the boundary line tan ν, which alongside r_{BL} and φ depends on a series of variables such as diameter of the rotating cylinder, filling degree, rotational speed, and flow properties of

the bed, is as yet unknown. A relation is derived for this below by using the balance of forces coupled with the mass balance.

Balance of Forces. Figure 3b illustrates the balance of forces on a differential element of the cascading layer with the length-related forces—gravity dF_G and inertia dF_I—acting at its mass center. The balance of forces in the level of the boundary plane produces

$$dF_F = dF_G \sin \eta - dF_I \cos \nu \tag{20}$$

The friction phenomenon on the boundary plane is modeled with the aid of Coulomb's law of solid body friction

$$dF_F = \mu dF_N \tag{21}$$

with μ characterizing the friction coefficient, which is further described in the following section. The normal force results from the balance of forces perpendicular to the boundary line

$$dF_N = dF_G \cos \eta + dF_I \sin \nu \tag{22}$$

After applying Eqs. 20 and 22 in Eq. 21 and converting the form, we obtain the following balance of forces from the previous considerations

$$dF_G(\sin \eta - \mu \cos \eta) = dF_I(\cos \nu + \mu \sin \nu) \tag{23}$$

The following applies for gravity

$$dF_G = dmg = \rho_b g t dx_{BL} \tag{24}$$

The flow motion causes inertia acting in the opposite direction, expressed as

$$dF_I = dm\bar{v}_x \frac{d\bar{v}_x}{dx_{BL}} \tag{25}$$

If the relations for the gravity (Eq. 24) and the inertia force (Eq. 25) are inserted in the balance of forces (Eq. 23), we obtain the motion equation for the rolling motion from this (Mellmann, 1989)

$$\bar{v}_x \frac{d\bar{v}_x}{dx_{BL}} - g \frac{\sin \eta - \mu \cos \eta}{\cos \nu + \mu \sin \nu} = 0 \tag{26}$$

To derive a relation for tan ν from Eq. 26, the mean velocity and its first derivation are needed.

Coupling with the Mass Balance. Applying the mass conservation law, a relation for the mean velocity was set up with Eq. 12. From this we derive

$$t \frac{d\bar{v}_x}{dx_{BL}} + \bar{v}_x \frac{dt}{dx_{BL}} + \omega r_{BL} \frac{dr_{BL}}{dx_{BL}} = 0 \tag{27}$$

Equation 27 thus corresponds to the continuity equation of the rolling motion. With the geometric relations 15 and 17 we obtain for the first derivation of the mean velocity after conversion

$$\frac{d\bar{v}_x}{dx_{BL}} = \frac{1}{t}\left[\omega r_{BL} \frac{\cos(\varphi + \nu)}{\cos \nu} - \bar{v}_x \tan \nu\right] \tag{28}$$

After inserting Eqs. 12 and 28 in Eq. 26 and introducing the dimensionless quantities

$$\rho_{BL} = \frac{r_{BL}}{R} \tag{29}$$

and

$$\delta = \frac{t}{R} = \rho_{BL} \sin \varphi - \cos \varepsilon \tag{30}$$

we obtain

$$\delta(\sin \eta - \mu \cos \eta) = \mathrm{Fr} \frac{1 - \rho_{BL}^2}{2\delta}\left[\rho_{BL} \frac{\cos(\varphi + \nu)}{\cos \nu} - \frac{1 - \rho_{BL}^2}{2\delta} \tan \nu\right](\cos \nu + \mu \sin \nu) \tag{31}$$

From the dimensionless representation, the Froude number, which is an important scaling criterion for the transverse bed motion, is expressed as

$$\mathrm{Fr} = \frac{\omega^2 R}{g} \tag{32}$$

The conversion of Eq. 31, applying trigonometric relations, ultimately leads to a square equation in tan ν (Mellmann, 1989)

$$a \tan^2 \nu + b \tan \nu + c = 0 \tag{33}$$

with the solution

$$\tan \nu = \frac{\sqrt{b^2 - 4ac} - b}{2a} \tag{34}$$

The parameters a, b, and c are calculated as

$$a = \mu\, \mathrm{Fr}(1 - \rho_{BL}^2)(1 - \rho_{BL}^2 + 2\rho_{BL}\delta \sin \varphi) \tag{35}$$

$$b = 4(\cos \Theta + \mu \sin \Theta)\delta^3 + \mathrm{Fr}(1 - \rho_{BL}^2)[1 - \rho_{BL}^2 + 2\rho_{BL}\delta(\sin \varphi - \mu \cos \varphi)] \tag{36}$$

$$c = 4(\sin \Theta - \mu \cos \Theta)\delta^3 - 2\,\mathrm{Fr}(1 - \rho_{BL}^2)\rho_{BL}\delta \cos \varphi \tag{37}$$

With this equation for tan ν the differential Eq. 19 for the boundary line can be solved. After this it is possible to calculate the velocity v_x and mass flow $\dot{M}_C$ in the cascading layer

from the geometry of the boundary line in accordance with Eqs. 6 and 10.

Coefficient of friction

To calculate the bed motion the dynamic angle of repose Θ of the bed and the friction coefficient μ are needed as material properties in accordance with the preceding equations. The dynamic angle of repose can be optically measured relatively easily. Measurements for friction values of rotating cylinder beds are not known, however. The flow properties of bulk materials are frequently determined with the aid of Jenike shear testers. For a given bulk density ρ_b of a material and thus consolidation stress, a yield locus results from the measurements. From this it is possible to determine the angle of internal friction ϕ, which is mostly constant for free-flowing bed materials. With this constant friction value $\mu = \tan \phi$, however, an unsymmetrical shape of the boundary line results from the equation system (Mellmann, 1989), which contradicts observations. Thus this frictional value cannot be used.

In this work, we assume that the coefficient of friction depends on the local position of the boundary line, as will be explained in the following. The vortex point W is the only point on the boundary line where there is no mass exchange between the plug flow region and the cascading layer (Figure 1). The transverse velocity there is thus zero. Therefore, only at the point W the friction can be described approximately with the Coulomb's law. Accordingly, the coefficient of friction is equal to the tangent of the angle of the plane to the horizontal, at which the solid body slips. This angle here is the dynamic angle of repose. Therefore, at the vortex point W the following condition must be satisfied

$$\mu(x_{BL} = 0) = \tan \Theta \tag{38}$$

Above the vortex point (from point W to point A, as shown in Figure 1), particles are transported from the plug flow region into the cascading layer. A velocity component is directed into the cascading layer, which obstructs the flowing of the particles. As a consequence, the coefficient of friction must increase with the distance to the vortex point, and the inclination angle of the boundary line must also increase so that the particle can flow further. At point A the condition

$$\mu(x_{BL} = -R \sin \varepsilon) = \tan(\Theta + \nu_A) \tag{39}$$

must be applied, where ν_A designates the inclination angle of the boundary line to the level bed surface (Figure 2).

Below the vortex point (from point W to point B), particles flow from the cascading layer into the plug flow region. A velocity component is directed into the plug flow region. The friction is therefore reduced and the inclination angle of the boundary line decreases until it reaches the value at point B.

Based on this conception, only the two angles Θ and ν_A are needed to characterize the coefficient of friction. The problem existing now is that μ and φ are coupled with each other (Eqs. 34–37), which makes the solution of Eq. 19 substantially difficult. However, it is shown that an approximation of the local friction coefficient with

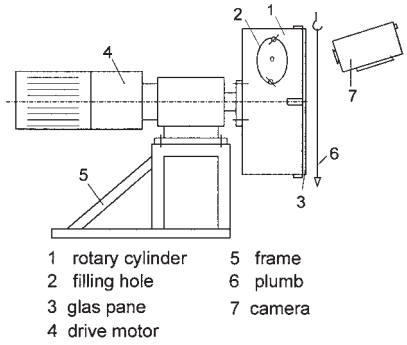

Figure 4. Experimental setup of the rotating cylinder.

$$\mu = \frac{\tan \Theta - \tan(\Theta + \nu_A)}{\sin \varepsilon} \frac{x_{BL}}{R} + \tan \Theta \tag{40}$$

is sufficient. This implies a linear variance of the coefficient of friction with the distance along the cascading layer, with $\mu = \tan \Theta$ at the vortex point W ($x_{BL} = 0$) and $\mu = \tan(\Theta + \nu_A)$ at point A ($x_{BL} = -R \sin \varepsilon$).

Initial condition

To solve the differential Eq. 19 for the boundary line, an initial condition at the top of the bed at point A is needed. If we insert $r_{BL}[\varphi = (\pi/2) - \varepsilon] = R$ here, as set out in simplified form in Figure 2, and hence the thickness of the cascading layer there, $t = 0$, we do not obtain any reasonable numerical solution. As high-resolution photos of the bed cross section in area A show, however, point A is not touched by particles. Rather, the distance between the top of the bed and point A becomes greater as the rotational speed increases. In the following a distance from the rotating cylinder wall of half a particle diameter is applied. Thus the initial condition is

$$\frac{r_{BL}}{R}(\varphi = \varphi_0) = 1 - \frac{d}{D} \tag{41}$$

with

$$\varphi_0 = \arcsin\left(\frac{\cos \varepsilon + \dfrac{d}{D}}{1 - \dfrac{d}{D}}\right) \tag{42}$$

With this initial condition the equation system described above can be solved numerically.

Comparison with Experiments

Experimental details

The experimental setup is shown schematically in Figure 4. Rotating cylinders of different diameters (D = 200, 300, and 500 mm) are used. A transparent glass pane (3) is secured at the head end of the cylinder for visual observation of the transverse bed motion. The rear wall is closed. To obtain undisturbed particle flow in the axial center of the cylinder, the rotating cylinders were produced with a length of $L/D > 0.3$. To avoid

Table 1. Bed Material Properties Measured in This Work

Material	Mean Particle Diameter d (mm)	Dynamic Angle of Repose Θ (°)
Glass beads	1	25
	2	27
	3	30
Sand	1.2	33
Steel ball	2.8	35
Steel cylinder	2	38
Activated carbon	0.55	35
	0.75	35
	8	39
Fertilizer pellets	3.4	40
Fermacell	0.8	42
	2	43
Grit	2.4	41
	3.5	41
	8	45

sliding motion a sand layer is stuck to the drum jacket on the inside. A geared motor allows infinitely variable speed change between 0.2 and 40 rpm. The filling hole (2) serves to adjust the filling degree. A plumb line (6) is fitted directly in front of the rotating cylinder so that it is possible to allocate the values to the perpendicular when measuring angles or measuring the bed cross section. The rotating axis is oriented horizontally. Photo lamps are used to illuminate the rotating cylinder.

The transverse bed motion was measured with the aid of photographic pictures of the bed cross section and video recordings of the particle motion on the bed surface. The cascading layer thickness $t(x_{BL})$, the profile of the boundary line $r_{BL}(\varphi)$, the dynamic angle of repose Θ, and the angle of slope at the start of the boundary line ν_A were determined with the aid of photographs. Similar measuring methods were also used in earlier studies by Tscheng (1978), Henein et al. (1983), Mellmann (1989), Evripidis (1991), and Blumberg (1995). Because of the friction of the bed at the glass pane (entraining effect), however, such measurements contain errors. Mellmann (1989) and Boateng (1993) previously pointed out the impact of the entraining effect.

The particle velocity at the bed surface was determined experimentally with the aid of a video camera (250 images/s). The video camera was aligned in such a way that a view of the entire bed surface was possible. Video films were taken in the undisturbed area of particle flow (in the axial center of the cylinder). By evaluating the individual images of the film, tracks of individual particles were followed and measured. By knowing the time interval of the images, the particle velocity could then be determined. Marks indicating the position of the rotating axis at the front glass pane and at the rear wall serve to measure the rotating cylinder radius in the scale of the image at both positions. This made it possible to determine the conversion factor image—original for measurements in the axial center of the drum.

Bed materials of different kinds and particle sizes are used in the experiments (Table 1). Experiments with activated carbon $d = 0.55$ mm were previously carried out in the earlier study of Mellmann (1989). The dynamic angle of repose Θ and the angle of slope at start of the boundary line ν_A were determined with the aid of photographs. For a certain material, Θ was found to be nearly independent of the rotation speed and filling degree in the range of rolling motion. This was also observed by Henein et al. (1983), Spurling (2000), and Ding et al. (2001b). Table 1 gives measured values of the angle Θ for materials investigated in this work. The angle ν_A is relatively difficult to measure. For this it is expedient to determine the inclination angle of the boundary line to the horizontal at the top of the bed η_A or the angle at the foot η_B (Figure 2), which can be measured optically. The following then applies for the inclination angle

$$\nu_A = \eta_A - \Theta \tag{43}$$

and

$$\nu_A = \Theta - \eta_B \tag{44}$$

This method was previously suggested by Brown and Richards (1970). For sand, for example, they stated values of $\eta_A = 50°$ and $\eta_B = 19°$. With the angle of repose for sand of about $\Theta = 33°$, the following applies for the angle of slope $\nu_A = 17°$ and $\nu_A = 14°$. The measurement of the angle η_A has an error attributed to the entraining effect of the front glass pane. This is caused by the adhesion friction between the glass pane and particles in the plug flow region, in which both move with the same velocity in the same direction. As a result, the boundary line is distorted in the upper part of the bed at the transition to the cascading layer. However, the measurement of the angle η_B in the lower part of the bed is more unproblematic. Here the particles roll with many times the velocity of the glass pane crossways to their motion direction in the cascading layer, so that as a result of the inertia of the particles the position of the boundary line at the transition to the plug flow region is influenced less strongly. It should also be noted that at very low rotational speeds there may be distortion of the boundary line.

According to our measurements, ν_A increases with Fr and f, as can be seen from Figure 5a for fertilizer pellets. The size ratio D/d imposes its influence as well (see Figure 5b). The smaller the ratio D/d, the higher is the value of ν_A if other parameters are constant.

Based on measurements with 15 different bed materials used in our experiments, we obtained an empirical equation for ν_A in the unit of degree

$$\nu_A = 0.32\Theta(1 + f) + 1800\sqrt{\frac{d}{D}}\,\mathrm{Fr}. \tag{45}$$

Equation 45 consists of two parts: the first dominant part considers the main influence variables filling degree f and dynamic angle of repose Θ (in degrees); the second part represents the dependency on the Froude number. It is assumed that ν_A increases linearly with Fr. The size ratio d/D is used as a correcting factor. Figure 6 shows the deviation of the approximated ν_A based on Eq. 45 from measurements for test materials used in the experiments. It can be seen that most of the points scatter near the line where approximated ν_A are equal to the measurements. It should be noted that further experiments must be carried out to verify Eq. 45 for other kinds of materials.

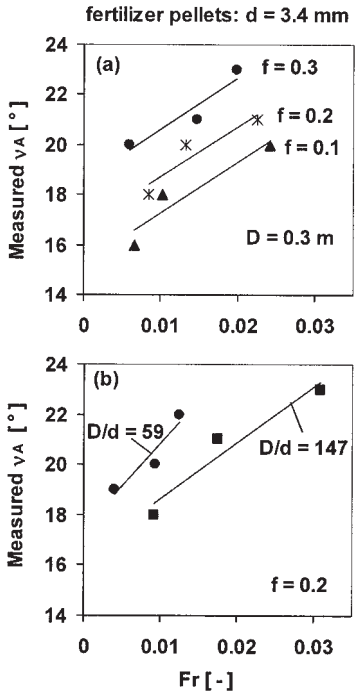

Figure 5. Measured values of ν_A for different Froude numbers (Fr), size ratios (D/d), and filling degrees (f).

Experimental results and discussion

In this part, calculated results from the model are compared to experimental data. To validate the model, measurements from the literature were used as well when parameters required for the calculation were available.

Measured and predicted shapes of the boundary line radius $r_{BL}(\varphi)$ for activated carbon at various filling degrees are compared in Figure 7. The shape of the boundary line was examined experimentally in an earlier study of Mellmann (1989). Because of the lack of corresponding measurements of ν_A, the value needed for the model calculation was obtained from Eq. 45. Solid lines correspond to model predictions. As shown in Figure 7, calculated results are in relatively good agreement with the measurements.

Figure 8 illustrates the thickness profile of the cascading layer in dimensionless form. Measurements from our experiments (Figure 8a) for steel balls ,$d = 2.8$ mm, and those from Orpe et al. (2001) (Figure 8b) for $d = 2$ mm are used to test the model. A dynamic angle of repose of $\Theta = 35°$ is assumed for the calculation for steel balls ($d = 2$ mm), as measured for steel balls ($d = 2.8$ mm) from our own experiments. According to the model, the cascading layer becomes thicker at higher filling degrees and larger Froude numbers, which is in good agree-

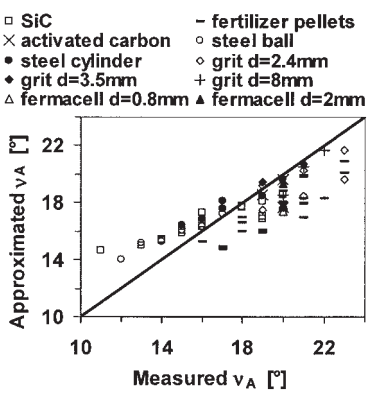

Figure 6. Approximated vs. measured values of ν_A.

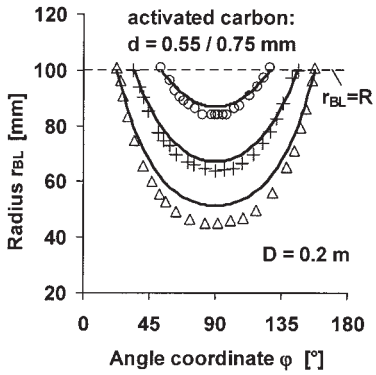

Figure 7. Shapes of the boundary line for activated carbon.

Symbols denote measured values from our own experiments: ○, $f = 0.05$, $d = 0.75$ mm, Fr = 0.00096; +, $f = 0.15$, $d = 0.55$ mm, Fr = 0.0035; △, for $f = 0.25$, $d = 0.55$ mm, Fr = 0.00096. Solid lines correspond to model predictions.

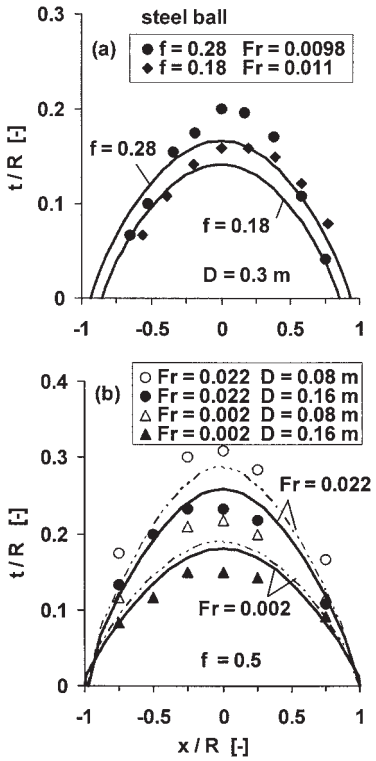

Figure 8. Measured and predicted profiles of cascading layer thickness for steel balls.

(a) Symbols denote measured values for $d = 2.8$ mm from our own experiments. Solid lines describe model predictions. (b) Measurements for $d = 2$ mm from Orpe et al. (2001). Solid lines correspond to model predictions for $D = 0.16$ m, dashed lines for $D = 0.08$ m.

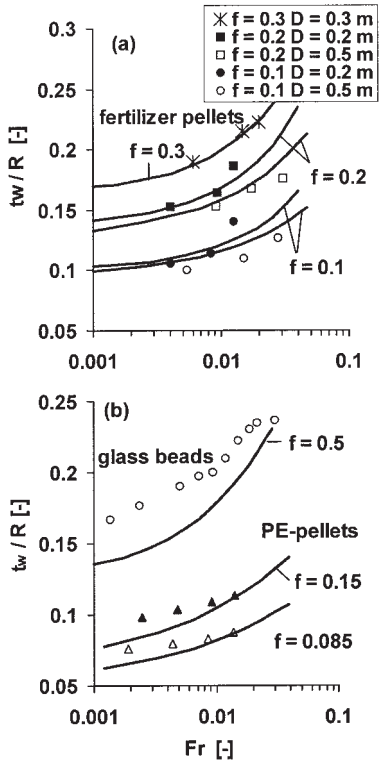

Figure 9. Measured and predicted thicknesses of the cascading layer t_w/R as a function of the Froude number.

Solid lines denote model predictions. (a) Measured values for fertilizer pellets (d = 3.4 mm) are from our own experiments. (b) Measured values for glass beads (d = 2 mm, D = 0.2 m, f = 0.5) are from Felix et al. (2002); for polyethylene (PE) pellets (d = 3.63 mm, D = 0.964 m, Θ = 25°) at filling degrees f = 0.15 (▲) and f = 0.085 (△) from Boateng (1993).

ment with the measurements. A maximum error of 20% (at position x/R = 0) is tolerable on considering the entraining effect of the front pane of the cylinders. It should be noted that numerous measurements are available in the work of Orpe et al. (2001). Here we select only measurements that are confined to the rolling regime. The empirical equation $\mathrm{Fr}_C = 2(d/D)$, from Blumberg (1995), can be used to estimate the critical Froude number Fr_C for the transition from rolling to cascading (Mellmann, 2001).

Figures 9 and 10 illustrate a series of measurements of the dimensionless thickness of the cascading layer at the vortex point $\delta_w = t_w/R$ as a function of the Froude number. Experimental data of different sources are involved here: for fertilizer pellets from our experiments, polyethylene pellets (PE) from Boateng (1993), glass beads from Félix et al. (2002), and Jain et al. (2002). For the calculation it is assumed that the glass beads used by the cited researchers have the same dynamic angle of repose as that given in Table 1. As Figure 9 shows, the model predicts well both the trend and the absolute values of the measurements with a maximum error about 18% for glass beads. However, as shown in Figure 10, the predicted results are much higher than the measured values for glass beads from Jain et al. (2002). It can be seen that the Froude numbers in their experiments are much smaller ($\mathrm{Fr} \leq 4.0 \times 10^{-4}$) than those used by other researchers ($\mathrm{Fr} \geq 1.0 \times 10^{-3}$, as shown in

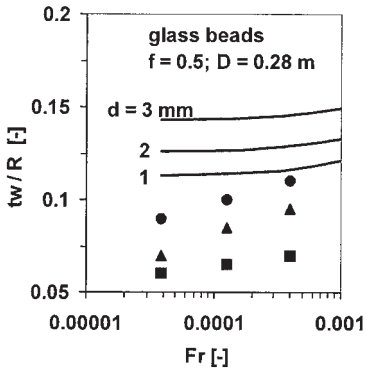

Figure 10. Measured and predicted thicknesses of the cascading layer t_w/R as a function of the Froude number.

Measurements for glass beads, d = 1 mm (■), d = 2 mm (▲), d = 3 mm (●), are from Jain et al. (2002). Solid lines are predictions of the model.

Figures 7–9). Using such small Froude numbers, it is unclear whether the motion is still in the range of rolling mode.

In Figure 11 distributions of the particle velocity at the surface $v_{x,S}$ are displayed by the dimensionless rolling path x_{BL}/R. Measured and predicted progressions for the sand frac-

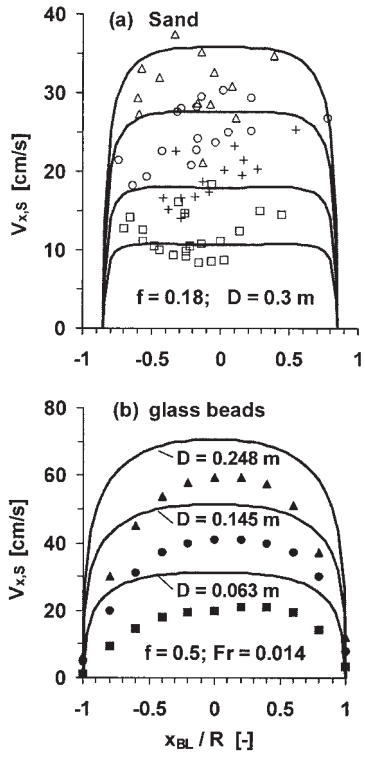

Figure 11. Measured and predicted surface velocity distributions.

(a) Measured values for sand, d = 1.2 mm, are from our own experiments: for Fr = 0.00022 (□), Fr = 0.00064 (+), Fr = 0.00166 (○), and Fr = 0.00311 (△). (b) Measurements are from Alexander et al. (2002) for glass beads d = 1.6 mm at similar Froude number (Fr = 0.014): for cylinders of D = 0.063 m (■), D = 0.145 m (●), and D = 0.248 m (▲); the corresponding rotation speeds are 20, 13, and 10.2 rpm, respectively. Solid lines describe model predictions.

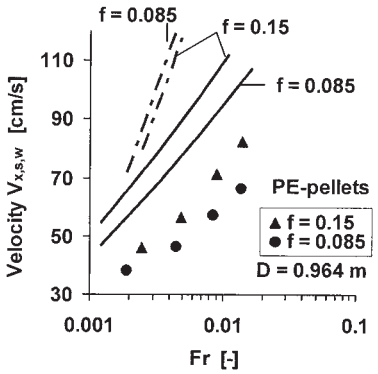

Figure 12. Measured and predicted surface velocities at mid-chord in dependency on the Froude number.

Measured values for PE pellets, $d = 3.63$ mm, are from Boateng (1993). Solid lines correspond to model predictions of this work; dashed lines are calculated results from the model of Elperin et al. (1998).

tion, $d = 1.2$ mm, under various Froude numbers are compared with each other in Figure 11a. The solid lines represent the predicted velocities. These were determined for the upper half of the bed and reflected in the middle of the bed ($x_{BL}/R = 0$). The measurements show a relatively strong scatter, which is attributable to the high turbulence in the cascading layer. Nevertheless, both the measurements and the model results show that the surface velocities increase with increasing Froude number. At the lowest Froude number, Fr = 0.00022, the velocity is nearly constant. In Figure 11b measurements from Alexander et al. (2002) are used to test the model, where the parameter is the cylinder diameter. According to the model, the velocity initially increases steeply in the vicinity of the wall and in the subsequent path it increases with very small gradients. In the middle of the bed the velocity attains a maximum. At small cylinder diameter ($D = 0.063$ m) the gradients are so small that the velocity progressions appear to be straight lines. This is in good agreement with experiments, except that the calculated values are slightly higher than the measured ones.

Figure 12 shows measurements of the surface velocity at mid-chord $v_{x,S,W}$ as a function of the Froude number by way of example for polyethylene pellets (PE), $d = 3.63$ mm (Boateng, 1993). The dashed lines represent results from the model of Elperin et al. (1998). The fitting parameter needed for their model was obtained by fitting the calculated cascading layer thickness to the measured value. Their model gives the mean velocity in the cascading layer. To calculate the values of the surface velocity, the cascading layer is assumed to have a linear velocity profile. The solid lines are predictions from the model of this work. Results show that both models can describe the trend of the surface velocity as a function of Froude number, although higher (this model) or much higher (Elperin's model) absolute values are predicted. According to the model of Elperin et al., the particle velocity decreases with increasing filling degree, which is, however, contrary to the measurements and the calculation of this model.

Conclusions

(1) A mathematical model was developed for the rolling bed motion in rotating cylinders. With it the influence of the cylinder geometry (diameter D) and the operating variables (filling degree f, rotation speed n) on the shape of the boundary line, the thickness of the cascading layer, the profiles of particle velocity, and mass flow rate can be predicted without introducing fitting parameters.

(2) The model is based on mass and force balances. The friction on the boundary plane between the cascading layer and the plug flow region is assumed to vary locally. Above mid-chord of the material bed the mass is transported into the cascading layer. As a consequence, the flowing of particles there is obstructed and thus the coefficient of friction increases. Meanwhile, the inclination angle of the boundary line must increase to keep the particles flowing. Below mid-chord of the bed the mass is transported out of the cascading layer so that the flowing of particles there is facilitated. The coefficient of friction and thus the inclination angle of the boundary line decrease.

(3) To describe the influence of the bed material, only the dynamic angle of repose Θ and the size ratio d/D (particle diameter to cylinder diameter) are needed.

(4) To describe the local profile of the friction coefficient the inclination angle of the boundary line at top of the bed ν_A is needed. This angle is dependent on the filling degree and the above mentioned two material properties, but only slightly on the Froude number. For this angle, a simple empirical equation derived from many experiments with about 15 different bed materials is given to approximate its value.

(5) With the model, measurements under particular experimental conditions (different filling degrees, cylinder diameters, rotation speeds, and types of bed material), which were reported by six different reports in the literature as well as from our own experiments, can be predicted. The thickness profile of the cascading layer and the distribution of the surface velocity, as well as their maximum values at the mid-chord of the bed were studied. The agreement of the theory with the experiments can be taken as good within the scope of the scattering of measured values.

Notation

a, b, c = coefficients according to Eqs. 35 to 37
d = particle diameter, m
D = diameter of cylinder, m
F_F = friction force, N
F_G = gravity, N
F_I = inertia, N
F_N = normal force, N
Fr = Froude number
g = gravitational acceleration, m/s^2
L = length of cylinder, m
m = mass, kg
$\dot{M}_C$ = mass flow rate in cascading layer, kg/s
$\dot{M}_P$ = mass flow rate in plug flow region, kg/s
r_{BL} = radius of a point on the boundary line, m
R = radius of cylinder, m
t = thickness of the cascading layer, m
t_w = thickness of the cascading layer at the vortex point, m
v_x = particle velocity in the cascading layer, m/s
$\bar{v}_x$ = mean particle velocity in the cascading layer, m/s
$v_{x,S}$ = particle velocity at the bed surface, m/s
$v_{x,S,W}$ = particle velocity at the bed surface at mid-chord, m/s
v_φ = particle velocity in the plug flow region, m/s
x, y = Cartesian coordinates, m, m
y_C = length coordinate in the cascading layer, m

Greek letters

δ = dimensionless thickness of the cascading layer
ε = fill angle, rad
ϕ = angle of internal friction, rad
φ = auxiliary angle $\varphi = \gamma - \pi$, rad
φ_0 = initial condition (the angle), rad
γ = polar coordinate (angle), rad
η = inclination angle of the boundary line to horizontal line, rad
η_A = inclination angle of the boundary line to horizontal line at top of the bed A, rad
η_B = inclination angle of the boundary line to horizontal line at foot of the bed B, rad
μ = coefficient of friction
ν = inclination angle of the boundary line to the bed surface, rad
ν_A = inclination angle of the boundary line to the bed surface at top the bed A, rad
Θ = dynamic angle of repose, rad
ρ_b = bulk density of the bed material, kg/m^3
ρ_{BL} = dimensionless radius of a point on the boundary line
ω = angular rotation speed, rad/s

Literature Cited

Alexander, A., T. Shinbrot, and F. J. Muzzio, "Scaling Surface Velocities in Rotating Cylinders as a Function of Vessel Radius, Rotation Rate, and Particle Size," *Powder Technol.*, **126**, 174 (2002).

Blumberg, W., "Selektive Konvektions- und Kontakttrocknung im Drehrohr," PhD Thesis, VDI Verlag, Düsseldorf, Germany (1995).

Boateng, A. A., "Rotary Kiln Transport Phenomena: Study of the Bed Motion and Heat Transfer," PhD Thesis, University of British Columbia, Vancouver, Canada (1993).

Boateng, A. A., and P. V. Barr, "Modelling of Particle Mixing and Segregation in the Transverse Plane of a Rotary Kiln," *Chem. Eng. Sci.*, **51**, 4167 (1996).

Bonamy, D., F. Daviaud, and L. Laurent, "Experimental Study of Granular Surface Flows via a Fast Camera: A Continuous Description," *Phys. Fluids*, **14**, 1666 (2002).

Brown, R. L., and J. C. Richards, *Principles of Powder Mechanics*, Pergamon Press, Oxford, UK (1970).

Ding, Y. L., R. N. Forster, J. P. K. Seville, and D. J. Parker, "Some Aspects of Heat Transfer in Rolling Mode Rotating Drums Operated at Low to Medium Temperatures," *Powder Technol.*, **121**, 168 (2001a).

Ding, Y. L., R. N. Forster, J. P. K. Seville, and D. J. Parker, "Granular Motion in Rotating Drums: Bed Turnover Time and Slumping–Rolling Transition," *Powder Technol.*, **124**, 18 (2002a).

Ding, Y. L., R. N. Forster, J. P. K. Seville, and D. J. Parker, "Segregation of Granular Flow in the Transverse Plane of a Rolling Mode Rotating Drum," *Int. J. Multiphase Flow*, **28**, 635 (2002b).

Ding, Y. L., J. P. K. Seville, R. N. Forster, and D. J. Parker, "Solids Motion in Rolling Mode Rotating Drums Operated at Low to Medium Rotational Speeds," *Chem. Eng. Sci.*, **56**, 1769 (2001b).

Elperin, T., and A. Vikhansky, "Kinematics of the Mixing of Granular Material in Slowly Rotating Containers," *Europhys. Lett.*, **43**, 17 (1998).

Evripidis, I., "Kombinierte Kontakt- und Konvektionstrocknung in einem Trommeltrockner," PhD Thesis, University of Karlsruhe, Karlsruhe, Germany (1991).

Félix, G., V. Falk, and U. D'Ortona, "Segregation of Dry Granular Material in Rotating Drum: Experimental Study of the Flowing Zone Thickness," *Powder Technol.*, **128**, 314 (2002).

Ferron, J. R., and D. K. Singh, "Rotary Kiln Transport Processes," *AIChE J.*, **37**, 747 (1991).

Gray, J. M. N. T., "Granular Flow in Partially Filled Slowly Rotating Drums," *J. Fluid Mech.*, **441**, 1 (2001).

Henein, H., J. K. Brimacombe, and A. P. Watkinson, "Experimental Study of Transverse Bed Motion in Rotary Kilns," *Metall. Trans. B*, **14B**, 191 (1983).

Jain, N., J. M. Ottino, and R. M. Lueptow, "An Experimental Study of the Flowing Granular Layer in a Rotating Tumbler," *Phys. Fluids*, **14**, 572 (2002).

Kelbert, F., and C. Royere, "Lateral Mixing and Heat Transfer in a Rolling Bed," *Int. Chem. Eng.*, **31**, 441 (1991).

Khakhar, D. V., J. J. McCarthy, T. Shinbrot, and J. M. Ottino, "Transverse Flow and Mixing of Granular Materials in a Rotating Cylinder," *Phys. Fluids*, **9**, 31 (1997).

Kohav, T., J. T. Richardson, and D. Luss, "Axial Dispersion of Solid Particles in a Continuous Rotary Kiln," *AIChE J.*, **41**, 2465 (1995).

Makse, H. A., "Continuous Avalanche Segregation of Granular Mixtures in Thin Rotating Drums," *Phys. Rev. Lett.*, **83**, 3186 (1999).

Mellmann, J., "Zonales Feststoffmassestrommodell für flammenbeheizte Drehrohrreaktoren," PhD Thesis, Technical University of Magdeburg, Magdeburg, Germany (1989).

Mellmann, J., "The Transverse Motion of Solids in Rotating Cylinders—Forms of Motion and Transition Behaviour," *Powder Technol.*, **118**, 251 (2001).

Mellmann, J., and E. Specht, "Mathematical Modelling of the Transition Behaviour between the Various Forms of Transverse Bed Motion in Rotating Cylinders," *Cement-Lime-Gypsum Int.*, **54**, 281, 380 (2001).

Orpe, A. V., and D. V. Khakhar, "Scaling Relations for Granular Flow in Quasi-Two-Dimensional Rotating Cylinders," *Phys. Rev. E*, **64**, 031302 (2001).

Perron, J., and R. T. Bui, "Rotary Cylinders: Solid Transport Prediction by Dimensional and Rheological Analysis," *Can. J. Chem. Eng.*, **68**, 61 (1990).

Perron, J., and R. T. Bui, "Rotary Cylinders: Transverse Bed Motion Prediction by Rheological Analysis," *Can. J. Chem. Eng.*, **70**, 223 (1992).

Rajchenbach, J., "Flow in Powders: From Discrete Avalanches to Continuous Regime," *Phys. Rev. Lett.*, **65**, 2221 (1990).

Spurling, R. J., "Granular Flow in an Inclined Rotating Cylinder: Steady State and Transients," PhD Thesis, University of Cambridge, Cambridge, UK (2000).

Tscheng, S. H., "Convective Heat Transfer in a Rotary Kiln," PhD Thesis, University of British Columbia, Vancouver, Canada (1978).

Manuscript received Jan. 22, 2003, and revision received Mar. 10, 2004.